CrystEngComm

PAPER

View Article Online
View Journal | View Issue

Cite this: *CrystEngComm*, 2018, **20**, 2010

Controlling the size of Pt nanoparticles with a cationic surfactant, C_nTABr†

Jongsu Seo, Siwon Lee, Bonjae Koo and WooChul Jung *

Received 29th December 2017,
Accepted 12th March 2018

DOI: 10.1039/c7ce02235b

rsc.li/crystengcomm

Aqueous-based colloidal synthesis using alkyltrimethylammonium bromide (C_nTABr), a cationic surfactant, has attracted much attention recently as a simple and facile method to fabricate size- and shape-tunable metal nanoparticles. Despite the many related studies, however, the underlying synthesis mechanism and the exact role of the cationic surfactant have not yet been clarified. Here, we report how the size of Pt nanoparticles varies by using a wide range of chain lengths (n = 10, 12, 14, 16, and 18) and concentrations (0.005 to 0.18 M) of C_nTABr in aqueous-based colloidal synthesis. Highly monodisperse Pt particles with a size between 8 and 26 nm were obtained and confirmed by TEM analysis. Significantly, unlike other surfactants, when C_nTABr with a small chain length was used, the particle size increased with the concentration, which is different from the typical particle growth behavior by other surfactants. The UV-vis spectroscopy analysis results show that the chemical affinity between real precursors and micelles generated in solution is an important factor in determining the size of the Pt nanoparticles. Based on this insight, we successfully demonstrated that the particle size is also controllable by modifying the critical micelle concentration with a KBr additive. Our results provide useful guidelines for nanoparticle synthesis using cationic surfactants.

Introduction

Metal nanoparticles (NPs) are of great scientific interest because they are, in effect, a bridge between bulk materials and atomic or molecular structures. Unlike bulk materials, their physical properties are strongly dependent on nanoscale particle dimensions and can be used in a wide range of industrial applications that require different properties.[1–4] Thus, it is critical to tailor the size and shape of metal NPs with a high level of precision.

The chemical reduction method has commonly been used to synthesize colloidal metal NPs due to the simplicity and handiness of a typical solution-based process. Over the past few decades, there have been many attempts to fabricate various nanoscale particle architectures by controlling synthetic variables, such as the type and concentration of a precursor, surfactant or capping/stabilizing agent.[1,2,4–11] Although many studies have been reported on how individual components added during the synthesis affect particle growth, reactions vary greatly depending on the component type, concentration, and other conditions of synthesis. Thus, understanding mechanisms and controlling particle size are still a challenge. When it comes to aqueous-based colloidal synthesis using ionic surfactants, more uncertainty exists regarding the coordination chemistry and the role of surfactants and counter-ions. As of now, there is no consensus on strategies to control the size of particles.

The aqueous-based colloidal synthesis using C_nTABr, a cationic surfactant, has attracted much attention as a simple and facile method that fabricates size- and shape-tunable metal NPs.[12–22] Unlike other surfactants including carbonyl groups, C_nTABr binds weakly to metal surfaces making it easy to regulate particle shape and preserve catalytically active sites.[12] In general, it is known that small NPs are obtained when the concentration of C_nTABr increases because the passivation by surfactants inhibits the growth of the particles. In contrast, there are also reports that C_nTABr increases particle size. For example, Bernadett Veisze, *et al.* observed that Pd particles grow as the relative amount of C_{14}TABr to K_2PdCl_4 precursor increases. However, their experiments were done with C_{14}TABr (n = 14) in a very limited concentration range.[14] To the best of our knowledge, there are few studies that explain the dependence of NP size in terms of a wide range of surfactant types and concentrations when using C_nTABr.[5,6,13,14,23]

In this study, to clarify the correlation between the surfactant concentration and particle size, we synthesized Pt NPs using cationic surfactants (C_nTABr), a K_2PtCl_4 precursor and $NaBH_4$ reducing agent. In particular, we observed how the size of the Pt NPs varies with a wide range of chain lengths (n = 10, 12, 14, 16, and 18) and concentrations (0.005 to 0.18

Department of Materials Science and Engineering, Korea Advanced Institute of Science and Technology (KAIST), 291 Daehak-ro, Yuseong-gu, Daejeon, 305-701, Republic of Korea. E-mail: wcjung@kaist.ac.kr; Tel: +82 42 350 3314

† Electronic supplementary information (ESI) available. See DOI: 10.1039/c7ce02235b

M) of C_nTABr. The physical and chemical properties of the synthesized Pt NPs were characterized by X-ray diffraction (XRD), X-ray photoelectron spectroscopy (XPS), transmission electron microscopy (TEM), and ultraviolet-visible spectroscopy (UV-vis). These observations revealed that the chemical affinity between real precursors and micelles generated in solution is an important factor in determining the size of Pt NPs. Based on this insight, we successfully demonstrated that the particle size is also controllable by modifying the critical micelle concentration (CMC) with a KBr additive.

Experimental

Materials

Potassium tetrachloroplatinate(II) (K_2PtCl_4, 99.9%, Pt 46.0%), (1-decyl)trimethylammonium bromide ($C_{10}TABr$, $C_{13}H_{30}BrN$, 98%), (1-dodecyl)trimethylammonium bromide ($C_{12}TABr$, $C_{15}H_{34}BrN$, 99%), (1-tetradecyl)trimethylammonium bromide ($C_{14}TABr$, $C_{17}H_{38}BrN$, 98%), (1-hexadecyl)trimethylammonium bromide ($C_{16}TABr$, $C_{19}H_{42}BrN$, 98%), potassium bromide (KBr, 99+%) and sodium borohydride ($NaBH_4$, 98%) were purchased from Alfa Aesar. (1-octadecyl)trimethylammonium bromide ($C_{18}TAbr$, $C_{21}H_{46}BrN$, 98%) were purchased from Sigma-Aldrich. All reagents used in the experiments were of analytic grade and used without further purification.

Synthesis of C_nTABr (n = 10, 12, 14, and 16) templated Pt NPs

Fig. 1 shows the overall synthesis process used to produce the Pt NPs.[24] A solution mixture of C_nTABr (48.5–291.2 mM, 37.5 mL) and K_2PtCl_4 (9.1 mM, 5 mL) was in a 100 mL round-bottomed flask and heated to 50 °C in an oil bath under stirring at 300 rpm until the appearance of the mixture changed from cloudy to transparent. This cloudy compound is known as the real precursor formed by coulombic interaction between $[C_nTA]^-$ and $[PtBr_4]^{2-}$ forming $[C_nTA]_2[PtBr_4]$.[14,17,25,26] Subsequently, an ice-cooled aqueous solution of $NaBH_4$ (500 mM, 3 mL) was added as a reducing agent. The hydrogen gases generated in the flask were then released through a needle by stabbing it into a rubber septum and leaving it there for 20 minutes. The aqueous solution was kept at 50 °C during the reaction for 24 h.

X-ray diffraction (XRD)

The crystal structures of the samples were identified by XRD using a RIGAKU D/Max-2500 with Cu-Kα irradiation at 40 kV and 200 mA with a scan rate of 4° per minute from 20° to 80°.

X-ray photoelectron spectroscopy (XPS)

The chemical nature of prepared Pt NPs were analysed by XPS using a K-alpha (Thermo Scientific, USA) under ultrahigh vacuum with a 400 μm-diameter beam of monochromatic X-ray source, Al Kα ($h\nu$ = 1486.6 eV) radiation. To get a detail information of oxidation state, high resolution XPS scans of Pt 4f were obtained.

Transmission electron microscopy (TEM)

To confirm the morphology of the Pt NPs, TEM images were obtained with a JEM 3010 (JEOL, Japan) operating at 300 kV. The solution was sampled without any size sorting process and dropped onto a carbon coated copper grid right after fabrication. A wetted grid was dried in air for a 1 day.

Ultraviolet-visible spectroscopy (UV-vis)

UV-vis was conducted with a SolidSpec-3700 (SHIMADZU, Korea) at room temperature. A solution mixture of surfactant and K_2PtCl_4 before adding the reducing agent was sampled after changing from cloudy to transparent at 50 °C. By holding the ratio of K_2PtCl_4 to C_nTABr, the type of surfactant was changed from n = 12 to 14 with and without KBr.

Result and discussion

To ignore the evolution of particle size according to the reaction time and focus only on the influence of the type and concentration of the surfactant, we first confirmed the minimum time required to obtain stable Pt NPs. Fig. S1† shows the average size of the Pt NPs *vs.* reaction time using 0.18 M $C_{16}TABr$. At the beginning of the reaction, the size of the particles sharply increases with time, but after approximately 15 hours they do not grow anymore and remain constant at 9 nm in diameter. Additionally, XRD data of the synthesized

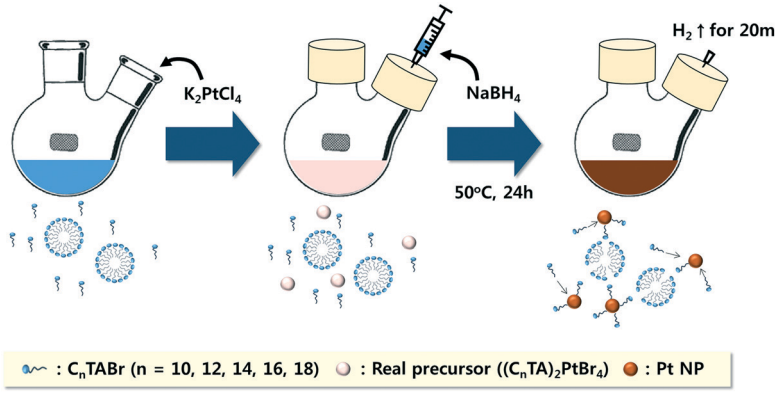

Fig. 1 Schematic flowchart of the synthetic procedure for the Pt nanoparticles (NPs).

Table 1 A table showing whether Pt nanoparticles are well synthesized

	0.005 M	0.01 M	0.04 M	0.08 M	0.12 M	0.18 M
C_{18}TABr	X	X	O	O	O	O
C_{16}TABr	X	X	O	O	O	O
C_{14}TABr	X	X	Δ	O	O	O
C_{12}TABr	X	X	Δ	O	O	O
C_{10}TABr	X	X	X	X	X	X

NPs in Fig. S2† show the same pattern with that of Pt, and the XPS data in Fig. S3† show the consistent chemical nature of Pt NPs compared with that previously reported in the literature.[27–29] Thus, in this study, all samples were synthesized with a sufficient reaction time of more than 24 hours.

Table 1 shows the results of synthesizing Pt NPs according to a wide range of C_nTABr species and concentrations. C_nTABr surfactants with five chain lengths (n = 10, 12, 14, 16, and 18) were used, and their concentrations were adjusted from 0.005 to 0.18 M. The solutions containing monodisperse Pt NPs were transparent dark brown color after synthesis, but under some conditions, large Pt agglomerates precipitated in the flask shown in Fig. S4.† Here, we define how uniformly the Pt particles are synthesized with the symbols O, Δ and X. O indicates that the particles are uniformly produced, whereas X means that the particles are not synthesized at all. Δ means that Pt NPs are generally well synthesized, but some aggregates precipitated under the flask. These results show that C_{18}TABr, which has the longest chain length, can form Pt NPs more easily in a wider concentration range. Given that a longer chain length is more hydrophobic, nanoparticles are generally easy to synthesize with hydrophobic surfactants.

TEM images of the synthesized Pt nanoparticles are shown in Fig. 2. Overall, monodisperse nanosized Pt particles were obtained, and their sizes and shapes differ slightly depending on the kind and concentration of the surfactant used in this study. Most of the particles have a cuboctahedra shape, and their size is slightly smaller or almost constant as the concentration of the surfactant increases. This is a generally reported trend indicating that C_nTABr acts as a passivation layer and inhibits particle growth. A more quantitative relationship between particle size and surfactant concentration is shown in Fig. 3. Interestingly, however, unlike other surfactants, when C_{12}TABr with the shortest chain length was used, cubic-shaped particles are obtained, and their size increases remarkably with an increasing C_{12}TABr concentration (note: the tendency of using C_{12}TABr is also consistent with the calculated NP size using Scherrer equation (Table S1†)). This tendency of the particle size to increase with the surfactant concentration is not generally known, and Bernadett Veisz *et al.* reported a similar phenomenon when synthesizing Pd NPs using C_{14}TABr.[14] They explained that as the concentration of the surfactant increases, the number of micelles, which are aggregates of the surfactants, increases thus inhibiting the diffusion of free surfactants to the particle surfaces. However, if the micelles merely interfere with the diffusion of free surfactants, very small Pt NPs should be formed

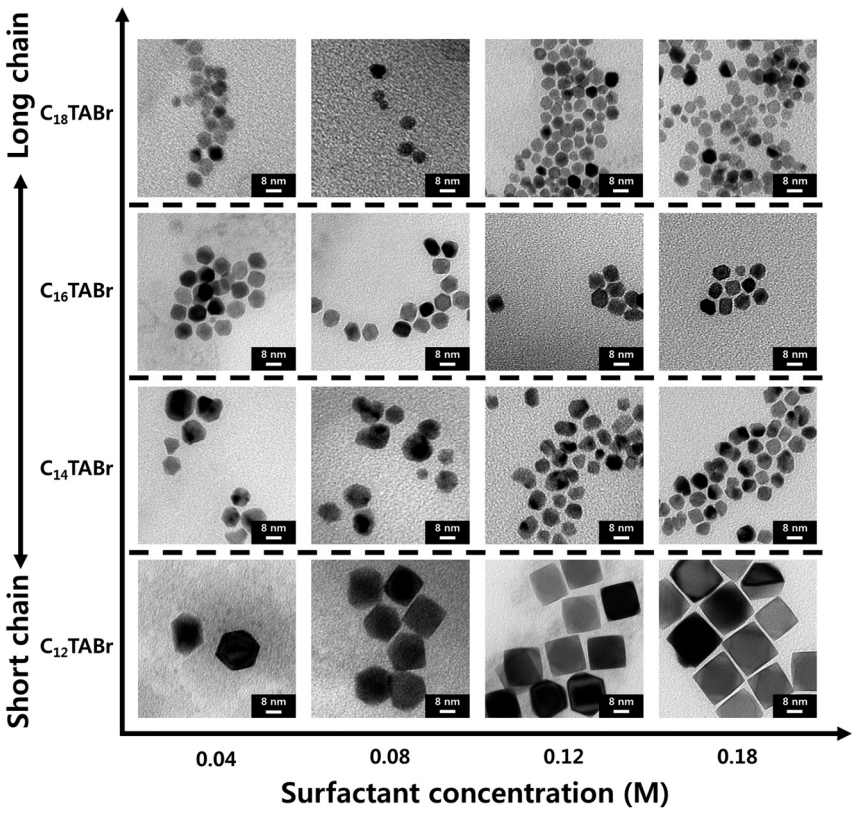

Fig. 2 TEM images of Pt nanoparticles prepared with various surfactant types and concentrations.

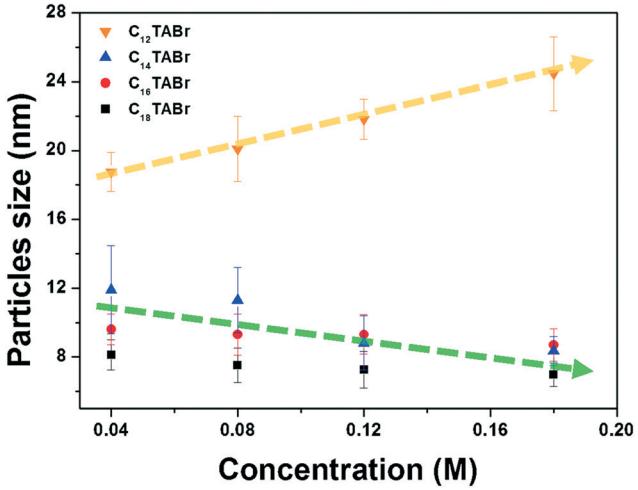

Fig. 3 The average particle size of the Pt nanoparticles prepared with various surfactant types and concentrations. The error bars were obtained by analyzing more than 100 particles for each sample.

near the CMC where most of the surfactants are not aggregated (Fig. S4(b)†). The CMC value of each surfactant is summarized in Table S2.†[30–34] Therefore, their explanations alone cannot fully interpret our observations when C_{12}TABr was used in this study.

In the case of Au NP synthesis, Zaheer Khan *et al.* reported that the organic complexes ($[C_{12}TA][AuCl_4]$) formed by the charge interaction between the surfactant and the precursor are solubilized into micelles, and the solubilized organic complexes directly participate in the formation of Au NPs when synthesizing Au NPs using C_{16}TABr and $HAuCl_4$.[18] Similarly, when the same C_nTABr and K_2PtCl_4 as those used in this experiment are used, an insoluble complex $[C_nTA]_2[PtBr_4]$ known as a real precursor is formed, and this real precursor is known to solubilize in a micelle system. Given these facts, it can be deduced that the chemical interaction between the real precursor and the micelle depending on the surfactant concentration, especially how many real precursors are dissolved in the micelle, has a role in the particle formation process. Therefore, in this study, we carried out UV-vis spectroscopy for the C_nTABr solutions to observe the real precursor and micelle states participating directly in the reaction (Fig. 4).

In the case of C_{12}TABr, which has a unique behavior, the peak intensity around 233 nm gradually increases with increasing surfactant concentrations. In contrast, for C_{14}TABr, which represents the other surfactants with longer chains, the peak is constant regardless of the concentration. In the case of the Pd NP synthesis, Bernadett Veisz *et al.* confirmed the interaction between the real precursor, $[C_{14}TA]_2[PdBr_4]$, and the micelles by varying the C_{14}TABr concentration followed by UV-vis spectroscopy. They said that the increase in the peak intensity at 251 and 342 nm is from the increasing interaction between the real precursor and the micelles because the number of micelles increase with increasing surfactant concentrations.[14] In addition to this, we confirmed that the an aqueous solution of only 0.08 M C_{12}TABr and 0.06 M KBr has no specific absorption band around 233 nm shown in Fig. 4(a).[21,22] Thus, the peak around 233 nm in our experiment is an indicator of the specific binding that expresses the interaction between the real precursor and the micelles. Therefore, we conclude that in the case of C_{12}TABr with the shortest chain length and a lack of hydrophobicity, $[C_{12}TA]_2[PtBr_4]$ is further solubilized into the micelles to increase the particle growth as the concentration increases. On the other hand, in longer chain surfactants where a sufficient interaction has already occurred between the real precursors and the micelles, fast particle size changes cannot be observed depending on their concentration.

To further confirm this conclusion, we observed the size of the synthesized Pt NPs by controlling the number of micelles in the solution using additives. KBr is an additive capable of effectively changing the CMC value, and its influence is as follows:[30]

$$\log \mathrm{CMC} = -0.55\{\log(0.0144 + [\mathrm{KBr}])\} - 2.83$$

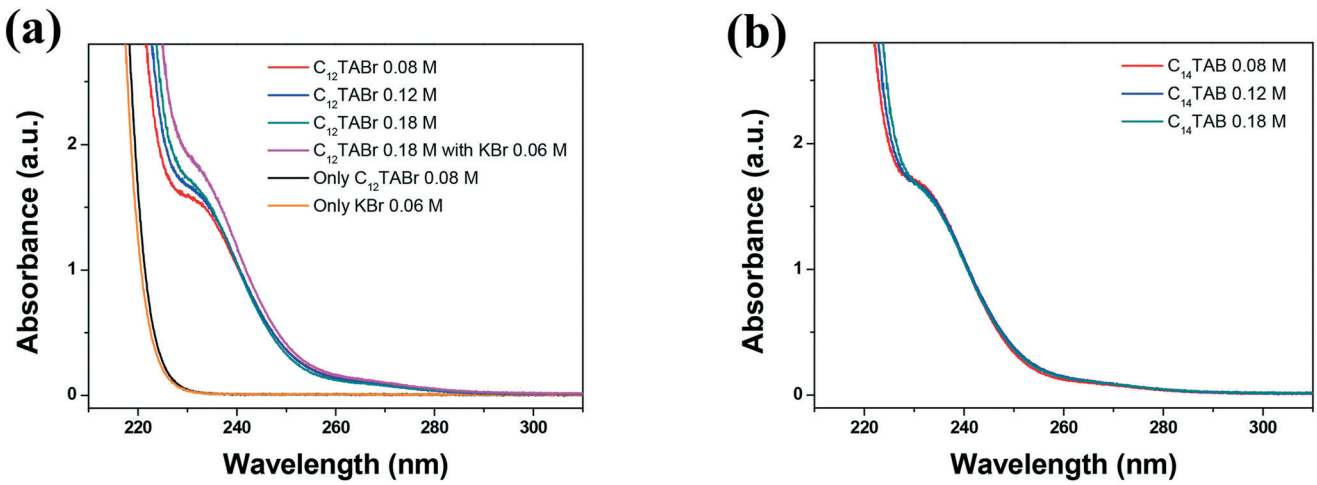

Fig. 4 UV-visible absorption spectra for the different reaction conditions using (a) C_{12}TABr and (b) C_{14}TABr.

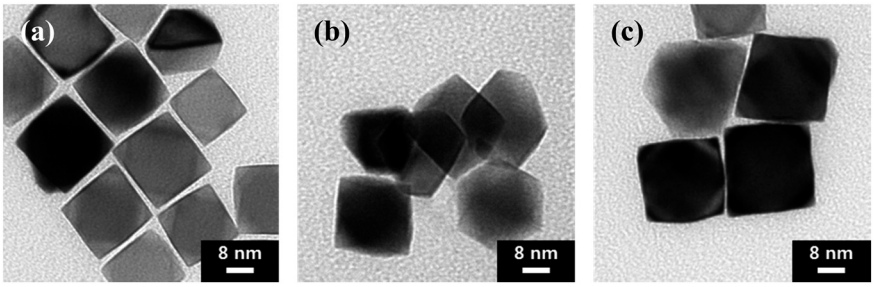

Fig. 5 TEM images of the Pt nanoparticles prepared with 0.18 M C_{12}TABr (a) without additive, (b) with 0.02 M KBr, and (c) with 0.06 M KBr.

It turns out that when KBr added to the same 0.18 M C_{12}-TABr solution is increased to 0, 0.02, and 0.06 M, respectively, the size of the Pt particles also grows gradually from 24.5 ± 2.1 nm to 27.3 ± 4.1 nm (Fig. 5). Furthermore, we confirmed that the addition of KBr also increases the peak intensity around 233 nm in the UV-vis (Fig. 4(a)). Conclusively, it can be understood that KBr decreases the CMC in the solution, and therefore, the number of micelles increases, and more organic complexes are solubilized, increasing the size of the synthesized Pt.

Conclusions

In this study, we synthesized Pt NPs using a cationic surfactant, C_nTABr. In particular, we observed how the size of the Pt NPs varies with the chain length and concentration of the C_nTABr over a wide range. When C_nTABr with n = 14 to 18 was used, cuboctahedra-shaped Pt particles were synthesized, and their size slightly decreased or remained almost constant with the surfactant concentration, as is generally known. In contrast, it was observed that C_{12}TABr forms cubic-shaped particles, and the particle size sharply increases as the concentration increases. Using UV-vis spectroscopy and the KBr additive, we succeeded in confirming that the chemical affinity between the organic complex formed in the solution and the aggregate of the surfactant, the micelle, is an important factor for Pt particle growth. These observations can provide useful guidelines for controlling the particle size and shape when cationic surfactants with a short chain length and insufficient hydrophobicity are used.

Conflicts of interest

There are no conflicts to declare.

Acknowledgements

This work was supported by Nano Material Technology Development Program through the National Research Foundation of Korea (NRF) funded by the Ministry of Science, ICT and Future Planning (NRF-2017M3A7B4049547) and by the Korea Institute of Energy Technology Evaluation and Planning (KETEP) and the Ministry of Trade, Industry & Energy (MOTIE) of the Republic of Korea (No. 20174030201590).

Notes and references

1 J. Chen, B. Lim, E. P. Lee and Y. Xia, *Nano Today*, 2009, **4**, 81–95.
2 M. Grzelczak, J. Pérez-Juste, P. Mulvaney and L. M. Liz-Marzán, *Chem. Soc. Rev.*, 2008, **37**, 1783–1791.
3 B. H. Kim, M. J. Hackett, J. Park and T. Hyeon, *Chem. Mater.*, 2013, **26**, 59–71.
4 M. Miyake and K. Miyabayashi, *Catal. Surv. Asia*, 2012, **16**, 1–13.
5 Y. Yin and A. P. Alivisatos, *Nature*, 2005, **437**, 664–670.
6 M.-P. Pileni, *Nat. Mater.*, 2003, **2**, 145–150.
7 P. Zhao, N. Li and D. Astruc, *Coord. Chem. Rev.*, 2013, **257**, 638–665.
8 Y. Xia, Y. Xiong, B. Lim and S. E. Skrabalak, *Angew. Chem., Int. Ed.*, 2009, **48**, 60–103.
9 Y. Xia, X. Xia, Y. Wang and S. Xie, *MRS Bull.*, 2013, **38**, 335–344.
10 B. L. Cushing, V. L. Kolesnichenko and C. J. O'Connor, *Chem. Rev.*, 2004, **104**, 3893–3946.
11 K. An and G. A. Somorjai, *ChemCatChem*, 2012, **4**, 1512–1524.
12 Y. Zheng, X. Zhong, Z. Li and Y. Xia, *Part. Part. Syst. Charact.*, 2014, **31**, 266–273.
13 T. Yonezawa, T. Tominaga and N. Toshima, *Langmuir*, 1995, **11**, 4601–4604.
14 B. Veisz and Z. Király, *Langmuir*, 2003, **19**, 4817–4824.
15 J. Tang, J. Huang and S.-Q. Man, *Spectrochim. Acta, Part A*, 2013, **103**, 349–355.
16 T. K. Sau and C. J. Murphy, *J. Am. Chem. Soc.*, 2004, **126**, 8648–8649.
17 H. Lee, S. E. Habas, S. Kweskin, D. Butcher, G. A. Somorjai and P. Yang, *Angew. Chem.*, 2006, **118**, 7988–7992.
18 Z. Khan, T. Singh, J. I. Hussain and A. A. Hashmi, *Colloids Surf., B*, 2013, **104**, 11–17.
19 D.-H. Chen and C.-H. Hsieh, *J. Mater. Chem.*, 2002, **12**, 2412–2415.
20 A. A. Athawale, P. P. Katre, M. Kumar and M. B. Majumdar, *Mater. Chem. Phys.*, 2005, **91**, 507–512.
21 S. Kundu and H. Liang, *Langmuir*, 2009, **26**, 6720–6727.
22 S. Kundu, D. Huitink and H. Liang, *J. Phys. Chem. C*, 2010, **114**, 7700–7709.
23 J. Zhuang, H. Wu, Y. Yang and Y. C. Cao, *Angew. Chem., Int. Ed.*, 2008, **47**, 2208–2212.

24 S. Lee, J. Seo and W. Jung, *Nanoscale*, 2016, **8**, 10219–10228.
25 K. Torigoe and K. Esumi, *Langmuir*, 1992, **8**, 59–63.
26 A. Kameo, A. Suzuki, K. Torigoe and K. Esumi, *J. Colloid Interface Sci.*, 2001, **241**, 289–292.
27 B. Malik, S. Anantharaj, K. Karthick, D. K. Pattanayak and S. Kundu, *Catal. Sci. Technol.*, 2017, **7**, 2486–2497.
28 S. Anantharaj, P. E. Karthik, B. Subramanian and S. Kundu, *ACS Catal.*, 2016, **6**, 4660–4672.
29 S. Anantharaj, K. Karthick, M. Venkatesh, T. V. Simha, A. S. Salunke, L. Ma, H. Liang and S. Kundu, *Nano Energy*, 2017, **39**, 30–43.
30 E. Rodenas, C. Dolcet, M. Valiente and E. C. Valeron, *Langmuir*, 1994, **10**, 2088–2094.
31 E. Rodenas, C. Dolcet and M. Valiente, *J. Phys. Chem. C*, 1990, **94**, 1472–1477.
32 A. C. Ribeiro, V. M. Lobo, A. J. Valente, E. F. Azevedo, M. d. G. Miguel and H. Burrows, *Colloid Polym. Sci.*, 2004, **283**, 277–283.
33 G. B. Ray, I. Chakraborty, S. Ghosh, S. Moulik and R. Palepu, *Langmuir*, 2005, **21**, 10958–10967.
34 J. Mata, D. Varade and P. Bahadur, *Thermochim. Acta*, 2005, **428**, 147–155.